Bulletin of the Geological Society of Finland, Vol. 94, 2022, pp 5–22 https://doi.org/10.17741/bgsf/94.1.001

# Timing of syn-orogenic, high-grade transtensional shear zone formation in the West Uusimaa Complex, Finland

Taija Torvela[1*] and Matti Kurhila[2]

[1]*University of Leeds, School of Earth and Environment, LS2 9JT, UK*
[2]*Geological Survey of Finland, PO Box 96, 02151 Espoo, Finland*

VERTAISARVIOITU
KOLLEGIALT GRANSKAD
PEER-REVIEWED
www.tsv.fi/tunnus

## Abstract

We present zircon and titanite U-Pb ages from granulite-facies transtensional shear zones and a greenschist facies strike-slip shear zone in the Karkkila-Vihti area, West Uusimaa. The zircon rim and titanite ages of c. 1815–1820 Ma from the transtensional shear zones constrain the evolution of the orogenic deformation from compression-dominated to syn-compressional lateral-escape within this part of the Fennoscandian shield while the zircon rim and titanite ages of 1790–1800 Ma give the timing of the late- to post-orogenic low-grade reactivation of the large-scale Somero-Karkkila fault zone. The new age data further constrain the timing of the changes in the crustal deformation style during orogenesis from i) compression-dominated to combined transpression - lateral stretching and escape, to ii) the late- to post-orogenic transition into retrograde conditions.

Keywords: West Uusimaa Complex, transtension, shear zones, age determinations, migmatite

*Corresponding author (e-mail: t.m.torvela@leeds.ac.uk)

Editorial handling: Niina Kuosmanen (e-mail: kuosmanen.niina@gmail.com)

## 1. Introduction

The co-existence of compressional and extensional/transtensional structures is commonly observed within orogenic belts. The syn-convergent extensional/transtensional structures are typically interpreted to result from i) syn- to late-orogenic collapse and/or orogen-parallel lateral escape due to crustal thickening and build-up of gravitational gradient (e.g. England & Houseman 1989; Fossen & Tikoff 1998); ii) presence of large-scale releasing bends between shear zones (e.g. Sanderson & Marchini 1984); or iii) a regional break in the convergence and crustal shortening (e.g. Skyttä & Mänttäri 2008).

Dating syn-orogenic deformation is challenging but in all of the above cases existing data suggest that the extensional/transtensional features form fairly late in the orogenic evolution. This is an important observation as it reflects the dynamic nature of orogens and how the boundary conditions change in time and space.

The overall evolution of the Svecofennian domain of Southern Finland is fairly well constrained, but the role of the syn-orogenic extensional/transtensional features is still debated (e.g. Skyttä & Mänttäri 2008; Torvela & Kurhila 2020). This is partly because of the paucity of both field observations and age data from such features, limiting the further understanding of the time-space development of this complex orogenic belt during the 1.85–1.80 Ga 'Fennian' convergence. Outcrop-scale boudinaged pegmatite and granite dykes, dated at c. 1.83–1.82 Ga, near Kisko-Orijärvi area were interpreted to reflect syn-Fennian crustal flattening and spreading (south of Sammatti in Fig. 1; Skyttä & Mänttäri 2008). This interpretation of large-scale flattening is slightly problematic as the convergence and significant crustal shortening, with large-scale folding and crustal thickening, evidently continued around this time: Torvela and Kurhila (2020) show that the migmatisation and crustal shortening were coeval, and that the thickening/folding of the partially molten crust was enabled by the rapidly crystallising, competent granitic sheets. However, extensional structures do facilitate some deformation within the shortening crust, particularly towards the later stages of an orogeny, and some extensional/transtensional shear zones have been interpreted in the field and from seismic reflection data near and north of Vihti (Fig. 1; Torvela et al. 2013). The pyroxene-bearing, transtensional shear zones of Torvela et al. (2013) that may accommodate lateral escape of the orogenic crust have not been previously dated, but we show in this paper that they too are broadly coeval with the other late-Fennian crustal features. We compile the evidence shown in this paper and in published literature into an interpretation of the role of the transtensional features as transient and local in nature. Our findings help to further constrain the regional changes in the crustal deformation style within the composite Svecofennian Domain, as well as the role of local features in accommodating overall crustal shortening.

## 2. Geological setting

The exhumed deep crust of the Palaeoproterozoic Svecofennian orogen consists of lower amphibolite facies to granulite facies rocks (Fig. 1; e.g. Ehlers et al. 1993; Väisänen & Hölttä 1999; Torvela & Annersten 2005). Most of the exposed rocks are migmatitic forming a c. E-W trending, c. 120 km wide 'Late-Svecofennian Granite-Migmatite belt' LSGM (after Ehlers et al., 1993). In southern Finland, the metamorphic peak conditions are c. 750–825°C and c. 4–7 kbar (e.g. Schreurs & Westra 1986; Väisänen & Hölttä 1999; Johannes et al. 2003; Mouri et al. 2005; Torvela & Annersten 2005; Torvela & Ehlers 2010a). This granulite-facies peak metamorphism is mostly undated but some geochronological data exist from migmatite leucosomes near Sammatti and Turku at c. 1825–1815 Ga (Väisänen et al. 2002; Mouri et al. 2005). The amphibolite facies LSGM schists and gneisses are also mostly migmatitic with peak conditions caluclated at c. 100–150°C and 0.3–2 kbar lower than in the granulite areas (Schreurs & Westra 1986; Väisänen & Hölttä 1999).

The Svecofennian orogen is multi-phased with at least two collisional episodes. Large amounts of juvenile crust formed in volcanic arcs between c. 1.92–1.86 Ga and accreted onto the Archaean craton in the present NE Fennoscandia (e.g. Lahtinen et al. 2005). This pervasive crustal deformation and stacking in present Southern Finland is now expressed mostly as recumbent/isoclinal folds (F1) with c. E-W striking axial planes, associated thrust sheets, and minor migmatisation (Fig. 2a; e.g. van Staal & Williams 1983; Bleeker & Westra 1987; Ehlers et al. 1993; Väisänen & Hölttä 1999). This first convergence

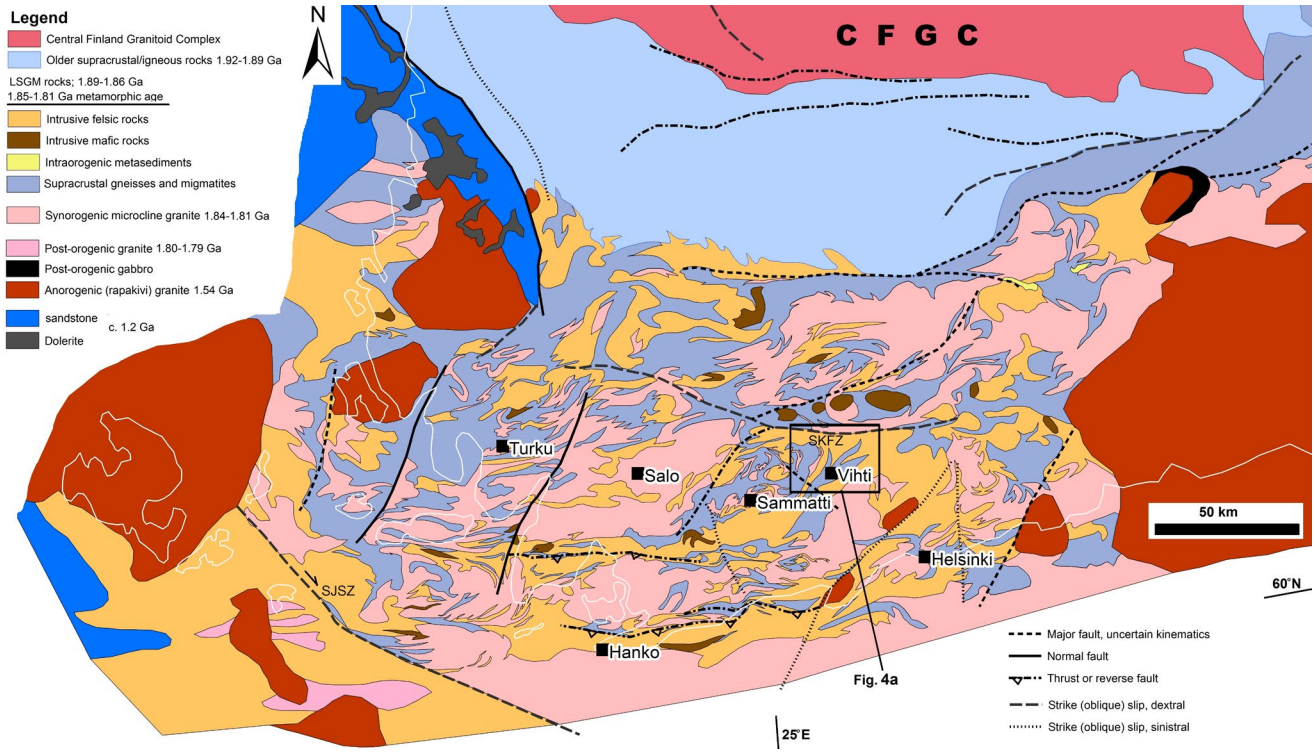


Figure 1. Simplified geological map of the Late Svecofennian Granite Migmatite belt, Southern Finland, and surrounding areas. The normal faults post-date the orogenic deformation, and many of the strike-slip zones show prolonged and complex kinematic histories (see text). SKFZ = Somero-Karkkila Fault Zone. Modified from Korsman et al. (1997), various 1:100 000 geological maps published by the Geological Survey of Finland, and from own field observations. Location of Fig. 4a is indicated with a rectangle.

was followed by a period of relative tectonic quiescence, possibly with minor crustal extension and rifting; however, this is poorly constrained from fluvial and shallow-water quartzitic sandstones deposited after c. 1.85–1.84 Ga at the presumed palaeomargin (Fig. 2b; Bergman et al. 2008; Lahtinen & Nironen 2010; Nironen & Mänttäri 2012). Either way, a second convergence started after c. 1.85–1.84 Ga (e.g. Lahtinen et al. 2005; Torvela et al. 2008). This phase (c. 1850–1800 Ma) refolded the F1 flat-lying crustal fabrics and recumbent folds into upright folds with E-W striking fold axes (F2; Fig. 2c; Torvela & Kurhila 2020). Particularly from c. 1825 Ma onwards, the deformation was synchronous with wide-spread low-P, high-T anatectic granite magmatism and migmatisation, metamorphism and formation of steep, local- to crustal-scale, strike-slip shear zones in the Svecofennian domain (e.g. Patchett & Kouvo 1986; Bleeker & Westra 1987; Ehlers et al. 1993; Lahtinen & Huhma 1997; Väisänen & Hölttä 1999; Väisänen & Mänttäri 2002; Hermansson et al. 2007; Högdahl et al. 2008; Torvela et al. 2008; Torvela & Ehlers 2010a, 2010b; Skyttä & Mänttäri 2008). This convergence phase, the 'Fennian orogen' (Lahtinen et al. 2005), is the focus of this paper. The Fennian phase, constrained by various authors to c. 1.85–1.80, is responsible for the main crustal configuration seen today in the study area, although there is evidence that the ~SSE-NNW convergence and compression continued until at least c. 1.79 Ga (e.g. Levin et al. 2005; Torvela et al., 2008; Torvela & Ehlers 2010b). Some authors suggests that a large-scale, distinct extensional phase or phases occurred around c. 1.83–1.81 Ga, before the final convergence, based on e.g. multiple stages of gold mineralization (Saalman et al. 2009); the presence of the internally underformed Veikkola

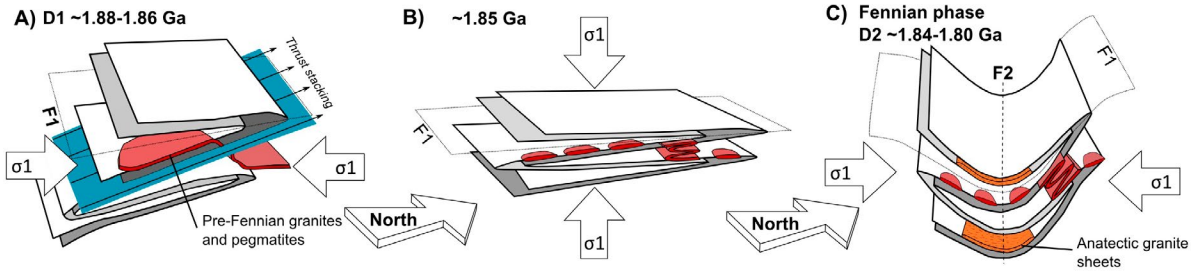


Figure 2. Schematic structural evolution of southern Finland during the composite Svecofennian orogen. a) Pre-Fennian phase (D1) with crustal stacking and recumbent folding, and minor migmatization and granite magmatism; b) a period of tectonic quiescence and relaxation enhancing the recumbent folds and mainly flat-lying crustal fabrics (D1 thrusts omitted for clarity); c) Fennian phase (D2) with upright folding, voluminous anatectic magmatism and migmatization, and formation of large strike-slip shear zones (not shown). Note the suggested deformation styles of both pre-Fennian and syn-Fennian anatectic granite sheets. See text for references.

granite complex near Vihti (Fig. 4a; Nironen & Kurhila 2008); and local extensional structures such as boudinaged pegmatites (Skyttä & Mänttäri 2008). However, Kurhila and Torvela (2020) show that despite voluminous partial melts in the crust, the convergence and crustal thickening was very much active during this age bracket, based e.g. on the fact that the 1.83 Ga Perniö granite is folded showing ~20% shortening after the full or partial solidification of the granite sheet.

It has been suggested that ~E-W compression caused by a convergence of the Amazonia from the west at c. 1.81–1.79 Ga, i.e. partly overlapping the Fennian orogenic phase, weakly modified the crustal fabrics within the Svecofennian domain, although evidence for this is debated (Fig. 2c; Lahtinen et al. 2005). Lahtinen et al. (2005) propose that this late E-W compression was responsible for the present dome-and-basin configuration of the LSGM. Alternative explanations have been brought forward: these include subvertical stretching during D2 (Fennian) compression (Cagnard et al. 2007); localised extensional/transtensional shearing around non-cylindrical folds (Torvela et al. 2013); or a mixture of 'cross-folding and diapirism' (Bleeker & Westra 1987).

Either way, fold interference patterns dominate the present geological maps, caused by the interaction of the early 'F1' folds (pre-1.86 Ga) and the later 'F2' folding episode during the Fennian phase. These composite folds generally display ~E-W striking steep F2 axial planes verging either south or north (more typically north; Torvela & Kurhila 2020). Besides folding, both transtensional and transpressional shear zones are observed, and some of these were reactivated as post-orogenic brittle faults (Väisänen & Skyttä 2007). The transpressional zones strike mostly W-E to NW-SE and are dominantly dextral, reflecting the Fennian N-S to NNW-SSE compression (e.g. the SJSZ and SKFZ in Fig. 1; e.g. Ehlers et al. 1993; Skyttä et al. 2006; Torvela and Kurhila 2020). A significant amount of geochronological and structural evidence suggests that the main deformation along most of these dextral shear zones took place c. 1.83–1.82 Ga, possibly as early as c. 1.85 Ga (e.g. Väisänen & Skyttä 2007; Torvela et al. 2008). Large-scale thrusting has been proposed to facilitate the deformation and crustal thickening during the Fennian phase (e.g. Lahtinen et al. 2005 and references therein; Levin et al. 2005; Skyttä et al. 2006). Whilst it is likely that Fennian (D2) thrusts exist, few have been identified in the field; the speculated low-angle, large-scale thrusts reported in the literature formed early, either during D1 in association with the large-scale recumbent F1 folds or early during D2 as they are now folded by the F2 folds and intruded by anatectic granites (van Staal & Williams 1983; Torvela and Kurhila 2020). The voluminous crustal-scale anatexis and migmatisation of the pre-Fennian rocks that

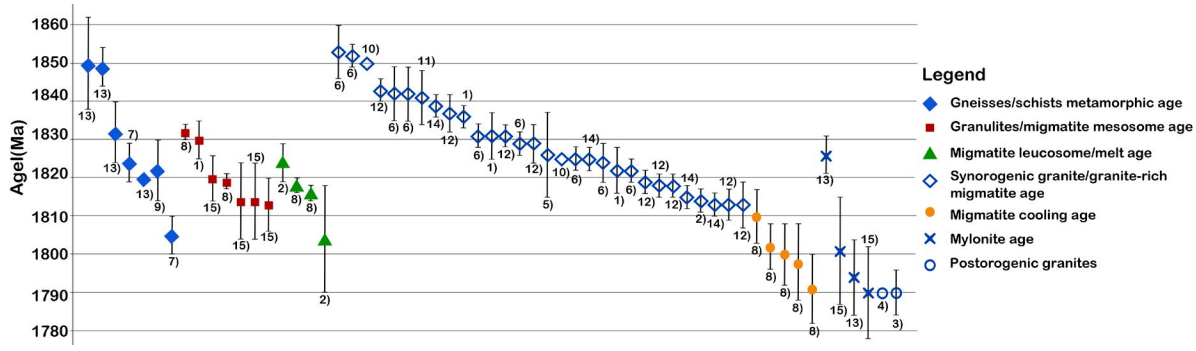


Figure 3. Compiled published age data from southern Finland, with error bars where available. Younger (post-1810–1805 Ma) ages are commonly related to cooling and lower amphibolite to greenschist facies deformation along discrete shear zones. Age data from 1) Suominen (1991); 2) Väisänen et al. (2002); 3) Ehlers et al. (2004); 4) Eklund and Shebanov (2005); 5) Jurvanen et al. (2005); 6) Kurhila et al. (2005); 7) Levin et al. (2005); 8) Mouri et al. (2005); 9) Skyttä et al. (2006); 10) Nironen and Kurhila (2008); 11) Pajunen et al. (2008); 12) Skyttä and Mänttäri (2008); 13) Torvela et al. (2008); 14) Kurhila et al. (2011); and 15) this study.

accompanied the Fennian deformation produced leucosomes giving syn-orogenic ages of c. 1.82 Ga (Fig. 3 and references therein). 'Microcline granite' bodies and sheets of variable thicknesses and lateral extents were emplaced throughout the Svecofennian Domain: their geochemical compositions strongly suggest they sourced from relatively local crustal partial melts (i.e. from the migmatites; e.g. Stålfors & Ehlers 2005). The ages of the microcline granites are consistently Fennian at c. 1.84–1.82 Ga (Fig. 3). At a crustal scale, the syn-orogenic granites are often folded but internally undeformed or show only weak cleavages at outcrop, unless within or in the vicinity of large shear zones (e.g. Torvela & Kurhila, 2020). The shear zones have been suggested to function as transport channels of at least some of the magmas (e.g. Selonen et al. 1996; Stålfors & Ehlers 2005).

Convergence continued at 1.81–1.79 Ga but during this time the strain is increasingly partitioned into steep, mylonitic to semi-brittle shear and fault zones deformed at lower amphibolite to upper greenschist facies conditions (e.g. Lindroos et al. 1996; Levin et al. 2005; Torvela & Annersten 2005; Torvela et al. 2008). Some small leucogranite intrusions show Late Fennian ages of ~1.81–1.79 Ga particularly in eastern Finland but, overall, the present erosion level of the crust had cooled significantly by c. 1.80 Ga (e.g. Suominen 1991; Johannes et al. 2003; Kurhila et al. 2011). Within e.g. the previously migmatised Sammatti area the metamorphic conditions had decreased to mid-amphibolite facies by c. 1.80 Ga (c. 600°C and 5 kbar; Mouri et al. 2005). No thrusting or large-scale folding occurred at this stage and extensional structures begin to overprint compressional fabrics between the steep crustal-scale shear zones (e.g. Torvela et al. 2013; Torvela & Kurhila 2020).

# 3. Methods

## *3.1. Sample description*

The main petrographic and mineralogical features of the samples that were dated are summarised in Table 1. The sampled rocks vary in mineralogy from clinopyrocene-rich tonalitic gneisses to Ca-rich, scapolite-clinopyroxene-calcite gneisses with an unknown protolith. Five rock samples were collected for age determinations from shear zones in the West Uusimaa area (Fig. 4).

Four of the samples (A2170, A2171, A2173, A2174) were collected from the extensional, pyroxene-bearing shear zones in the 'Karkkila granulite dome' within the West Uusimaa complex WUC (see Torvela et al. 2013 for details regarding the nature of these shear zones and e.g. Schreurs

Table 1. Summary of mineralogies and textures of the dated rock samples from Vihti area, S Finland. Abbreviations: qtz=quartz; plg-plagioclase; kfs=K-feldspar; bt=biotite; hbl=hornblende; aug=augite; ca=calcite; chl=chlorite; ti=titanite; sca=scapolite. See Fig. 7 for location map and sample photos.

| | Sample number | Sample location coordinates (YKJ) | Description |
|---|---|---|---|
| Pyroxene granulites (shear zones) | A2170 (004-09) | 3351484, 6713787 | Mineral assemblage: Plg-qtz-aug-kfs-sca-ca-ti. Very strongly foliated (090/35N), relatively equigranular, medium-grained ti-rich gneiss. Weak mineral lineation c. 055/28NE. Minor chloritization of aug. |
| | A2171 (007-09) | 3354612, 6714227 | Mineral assemblage: Plg-qtz-aug-kfs-sca-ca-ti. Very strongly foliated (090/22N), relatively equigranular, medium-grained ti-rich gneiss. Banding observed with mm-scale feldspar-rich layers within the foliation. Minor chloritization of aug. |
| | A2173 (004-10) | 3352500, 6709300 | Mineral assemblage: Plg-qtz-kfs-aug-ti. Strongly foliated (018/64E), relatively equigranular, medium-grained ti-rich gneiss. Weak mineral lineation c. 120/50SE. Minor chloritization of aug locally. |
| | A2174 (007-10) | 3352365, 6705224 | Mineral assemblage: Plg-qtz-kfs-aug-ca-ti with retrograde bt and chl. Strongly foliated (042/42SE), relatively equigranular, medium-grained ti-rich gneiss. Mm- to cm-scale layering with more aug-rich bands separated by feldspar-rich bands. Pegmatite granite dykes cutting the outcrop. |
| Mylonite | A2175 (014-10) | 3334245, 6719439 | Mineral assemblage: Plg-qtz-chl-hbl-kfs-ti. A ti-rich mylonite within the Somero-Karkkila fault zone. Very fine grained, relatively equigranular; randomly orientated plagioclase laths at micro-scale but strong foliation at macro-scale (070/70S). Hbl extensively chloritized. Dextrally asymmetric folding within the foliation at outcrop. |

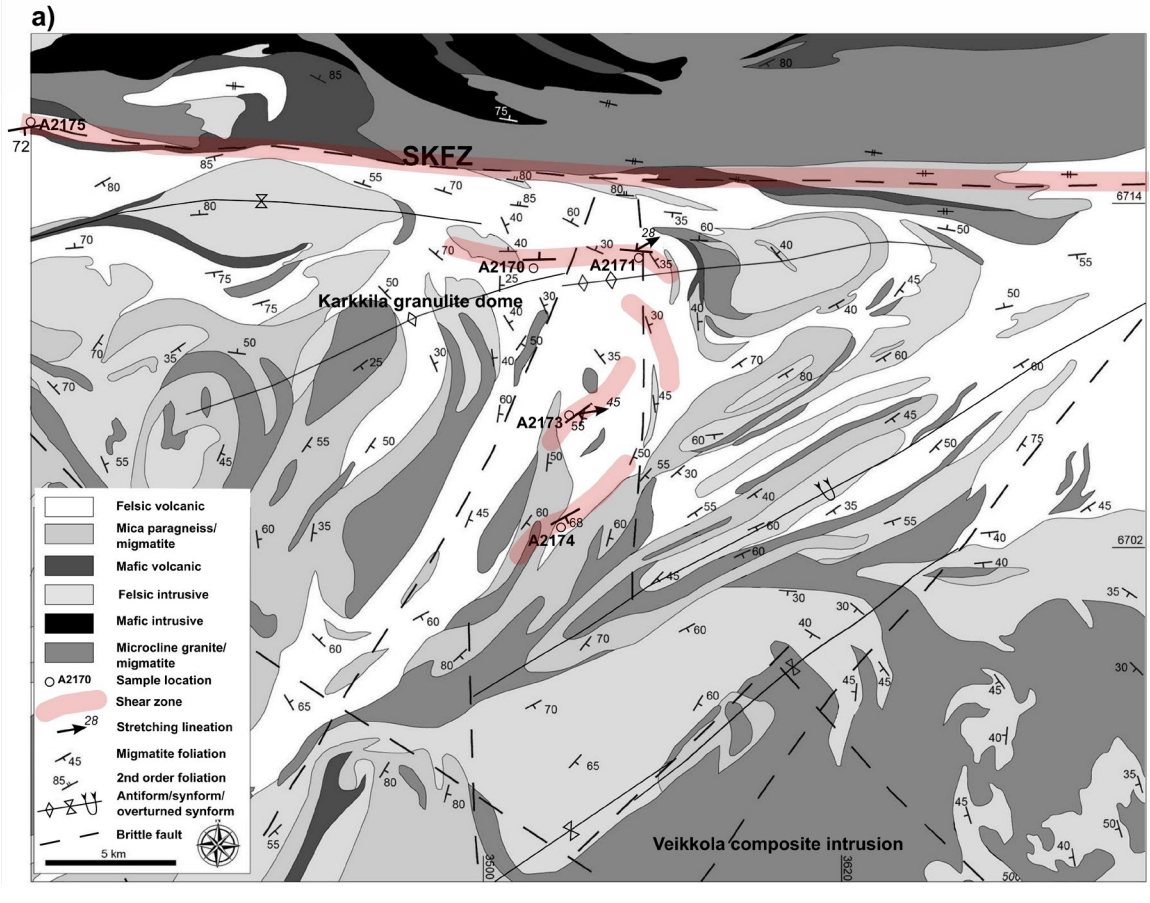

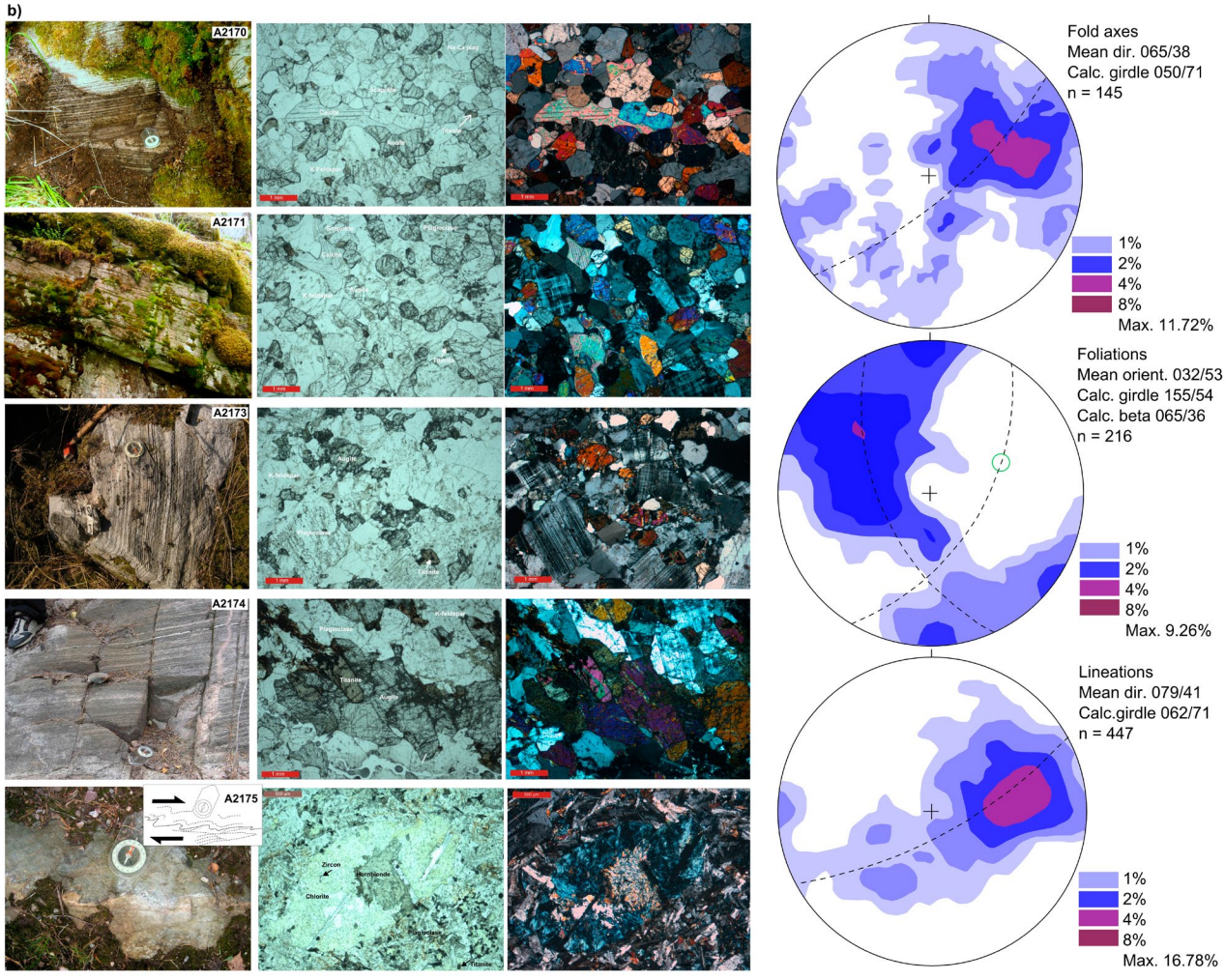


Figure 4. a) Geological map of the Karkkila granulite dome and surrounding areas, with sample locations for age determinations. The Somero-Karkkila Fault Zone S-KFZ is not well studied but our observations suggest it to be a long-lived fault zone with ductile (gneissose) precursor overprinted first by a greenschist facies semi-ductile shearing phase and, later, brittle faulting; the age determination sample of this study represents the semi-ductile deformation phase. b) Outcrop photos of the sample locations in a) and representative thin section photographs. c) Summary of structural data in the Vihti-Karkkila area illustrating the overall structure of the crustal fabric. Equal angle, lower hemisphere projections plotted using GEOrient v. 2.4.5 (modified after Torvela & Kurhila, 2020).

& Westra 1986 and Mouri et al. 2005, for general discussion of the metamorphism within the WUC). The px-bearing shear zones are defined by extremely regular, straight foliation at outcrop (Fig. 4b), the individual mm- to cm-thick layers composed of alternate clinopyroxene and scapolite-rich vs -poor intervals. The clinopyroxene-scapolite assemblage is compatible with granulite-facies temperatures (>800°C; e.g. Goldsmith & Newton 1977). The shear zones are up to a few hundred metres thick; the boundaries of the shear zones are diffuse and often covered by Quaternary deposits so the exact width is difficult to determine. Along strike, the shear zones are discontinuous and can be followed for up to a few kilometres after which they seem to die out into the migmatitic foliation; again, their exact extents are difficult to determine with precision due to the diffuse nature of the boundaries and the overburden. In thin section, The individual crystals from the granulite shear zones

commonly show very little internal strain, and the grain boundaries are typically relatively straight: we interpret this, together with the clinopyroxene-scapolite assemblage, to suggest that the rocks were at very high temperatures and quite probably partially molten at the time of the shearing (Fig. 4b). The titanite and zircon are intimately associated with the high-temperature crystals and fabric in thin section. Locally, medium-temperature deformation microstructures such as grain-boundary bulging, grain boundary migration and sub-grain rotation can, however, be observed to overprint the high-temperature fabrics, and some samples show signs of retrograde metamorphism (chloritization; Fig. 4b).

The fifth sample (A2175) was taken from a sheared metavolcanic rock within the sub-vertical Somero-Karkkila shear zone SKFZ (Fig. 4a, b; Table 1). The mineral assemblage defining the foliation and associated with the titanite and zircon (hornblende, plagioclase) suggests medium-grade conditions during shearing; significant retrograde chloritisation is seen to affect the hornblende (Fig. 4b, Table 1).

The samples were crushed and the heavy fractions (3.3–3.6 g/cm$^3$ and >3.6 g/cm$^3$) separated first with a shaking table, then heavy liquids. The zircons were hand-picked for analysis and mounted on epoxy pucks. The analysed zircons in all samples are mostly prismatic, rather stubby, euhedral, showing zoning of grain cores in the backscattered electron (BSE) images, whilst the rims are mostly unzoned (Fig. 5a). Some grains are anhedral and rounded, without clear zoning. Spot analyses were made both in the cores and the rims of the zircons, although in many zircons the rims were too narrow for the laser beam, or were missing, presumably lost during sample preparation. Many zircons also are fractured and affected by metamictisation; Fig. 5a). The titanite grains in all samples are relatively rounded and homogeneous although some show weak, irregular zoning (Fig, 5b). The spot analyses were made at locations with minimal zoning.

## 3.2. U-Pb geochronology

The dating was done in several sessions using a Nu Plasma HR multicollector ICPMS at the Geological Survey of Finland in Espoo. The analysed zircon and titanite grains were selected based on the BSE images (Fig. 5). The LA-ICP-MS analytical technique was very similar to that described by Rosa et al. (2009) except that a Photon Machine Analyte G2 laser microprobe was used. Samples were ablated in He gas within a HelEx ablation cell (Müller et al. 2009). The He aerosol was mixed with Ar (gas flow= 0.8 l/min) prior to entry into the plasma. The gas mixture was optimized daily for maximum sensitivity. All analyses were made in static ablation mode. Ablation normal conditions were: beam diameter: 20 μm for zircon and 30 μm for titanite; pulse frequency 5 Hz; and beam energy density 0.55 J/cm$^2$. A single U–Pb measurement included 30 s of on-mass background measurement, followed by 60 s of ablation with a stationary beam. Masses 204, 206 and 207 were measured in secondary electron multipliers, and 238 in the extra high mass Faraday collector. The geometry of the collector block does not allow simultaneous measurement of $^{208}$Pb and $^{232}$Th. Ion counts were converted and reported as volts by the Nu Plasma time-resolved analysis software. $^{235}$U was calculated from the signal at mass 238 using a natural $^{238}$U/$^{235}$U=137.88. Mass number 204 was used as a monitor for common $^{204}$Pb. The contribution of $^{204}$Hg from the plasma was eliminated by on-mass background measurement prior to each analysis. In an ICPMS analysis, $^{204}$Hg originates mainly from the He supply. The observed background counting-rate on mass 204 was ca. 1200 (ca. $1.3\times10^{-5}$ V), and has been stable at that level over the last years.

Age related common lead (Stacey & Kramers 1975) correction was used when the analysis showed common lead contents above the detection limit. Signal strengths on mass 206 were typically > $10^{-3}$ V, depending on the uranium content and

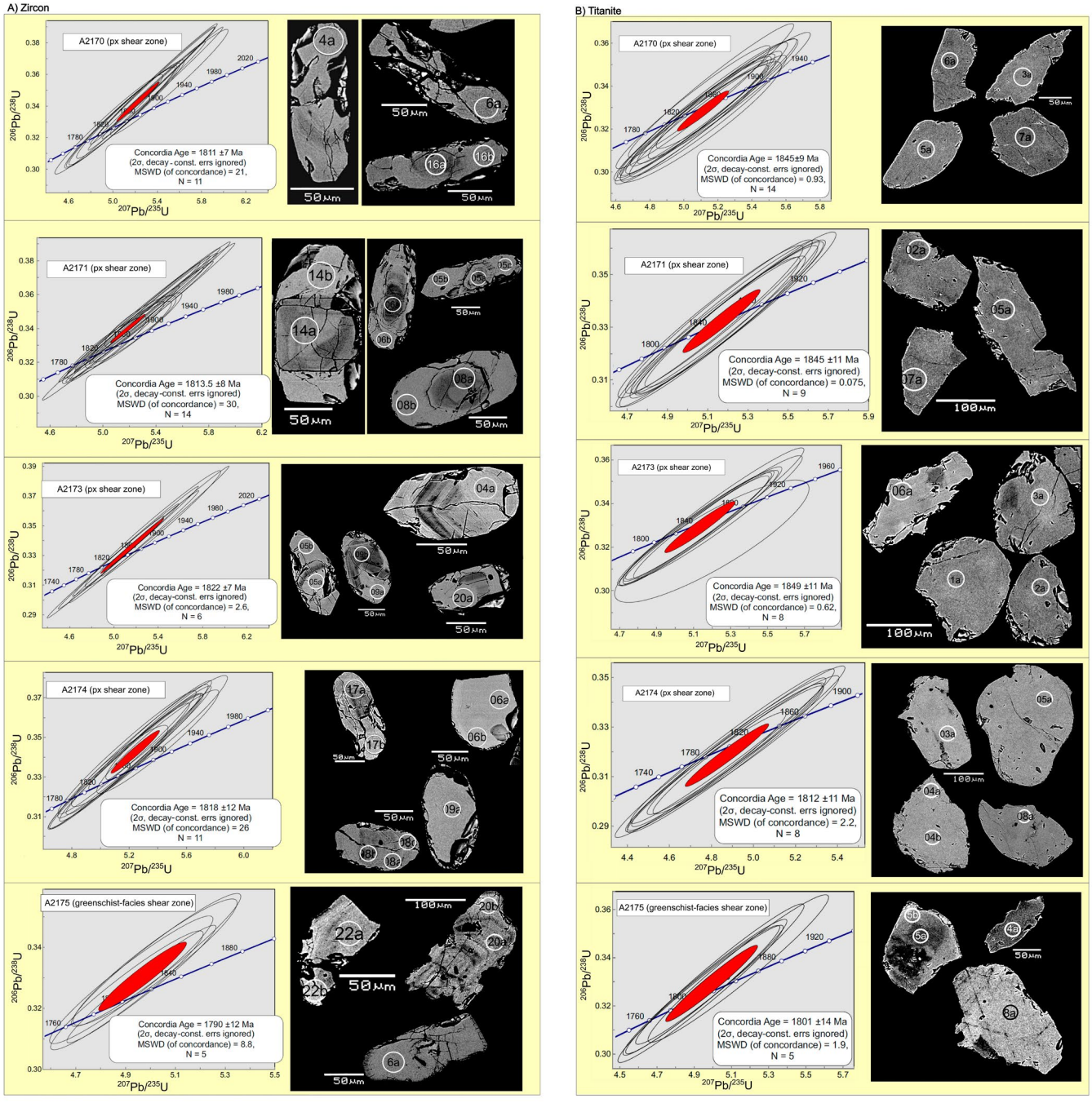


Figure 5. 206Pb/238U vs. 207Pb/235U concordia plots for the dated samples. All error ellipses are 2σ. a) Concordia plots and representative BSE images of the dated zircons; b) Concordia plots and representative BSE images for the dated titanites. The analysis data of the numbered analysis spot numbers in all images can be found in Electronic Appendix A.

age of the zircon. Two calibration standards were run in duplicate at the beginning and end of each analytical session, and at regular intervals during sessions. Raw data were corrected for background, laser induced elemental fractionation, mass discrimination and drift in ion counter gains and reduced to U–Pb isotope ratios by calibration to concordant reference zircons of known age, using protocols adapted from Andersen et al. (2004) and Jackson et al. (2004).

For the zircon analyses, standard GJ-01 (609 ± 1 Ma; Belousova et al. 2006) and an in-house standard A1772 (2712 ± 1 Ma; Huhma et al., 2012) were used for calibration. An in-house sample A382 was used for quality control (1877 ± 2 Ma, Patchett & Kouvo 1986; Huhma et al. 2012). The concordant age offset of this control sample does not exceed 0.5%. For titanite analyses, in-house standards A958 (1783 Ma; Hiltunen 1982) and A1772 (2598 Ma, unpublished) were used for calibration, and in-house sample A1756 (1857 Ma, unpublished) was used for quality control. The calculations were done off-line, using an interactive spreadsheet program written in Microsoft Excel/VBA by T. Andersen (Rosa et al. 2009). To minimize the effects of laser-induced elemental fractionation, the depth-to-diameter ratio of the ablation pit was kept low, and isotopically homogeneous segments of the time-resolved traces were calibrated against the corresponding time interval for each mass in the reference zircon/titanite. To compensate for drift in instrument sensitivity and Faraday vs. electron multiplier gain during an analytical session, a correlation of signal vs. time was assumed for the reference zircons/titanite. A description of the algorithms used is provided in Rosa et al. (2009). Plotting of the U-Pb isotopic data and age calculations were performed using the Isoplot/Ex 3 program (Ludwig 2003). All the ages were calculated with 2σ errors and without decay constant errors (Fig. 5). Decay constants of Steiger & Jäger (1977) were used. Data-point error ellipses in the figures are at the 2σ level.

# 4. Results

The derived ages (and their interpretations) are summarised in Table 2 and Fig. 5. The zircon and titanite U-Pb isotope data are collected in Appendix A. See the tables and figures when U concentrations, ages, individual spot ages, etc. are concerned. High common Pb data points (>5%) were discarded from age calculations (Appendix A). Some analyses were discarded because of inclusions and other internal heterogeneities resulting in large changes in Pb/U ratios in the course of the spot analysis.

Samples A2170, A2171, A2173, and A2174 from px-granulite shear zones show both older ages (mostly from zircon cores and rounded grains) and younger ages from zircon rims and from titanites. The older concordant ages from these samples combined cluster around 1946±15 Ma, 1908±6 Ma, 1911±19 Ma and 1849±17 Ma, for zircon cores, and around 1845–1850 Ma for titanite samples A2170, A2171 and A2173 (Table 2 and Electronic Appendix A). The zircon rims show systematically younger ages of 1811–1822 Ma, and one titanite sample (A2174) shows a younger age of 1812±11 Ma (Fig. 5).

Sample A2175 from the greenschist facies sheared metavolcanic rock within the S-KFZ shows an older zircon core age of 1874±17 Ma and a younger rim age of 1790±12 Ma; titanite from this sample yield an age of 1801±14 Ma (Fig. 5).

SEM images show many of the titanite grains to be internally heterogeneous, but a significant number of grains were reasonably homogeneous (Fig. 5b). The spot analyses were aimed at the more homogeneous grains and areas. The obtained ages show limited spreading, indicating that the analysed spot areas are isotopically reasonably homogeneous.

Table 2. Summary of U-Pb age determinations from Vihti area, southern Finland (Fig. 2). See text for discussion on age interpretations.

| | Sample number | Zircon morphology | Zircon U-Pb ages (Ma) Core | Rim | Titanite U-Pb age (Ma) |
|---|---|---|---|---|---|
| Pyroxene granulites | **A2170** | Cores zoned prismatic, or homogeneous; Rims homogeneous | **1946±15** | **1811±7** | **1845±9** |
| | *Age interpretation* | | *Mixed protolith age* | *Late D2* | *Poss. early D2* |
| | **A2171** | Cores mostly zoned prismatic, some homogeneous; Rims homogeneous | **1908±6** | **1814±8** | **1845±11** |
| | *Age interpretation* | | *Mixed protolith age* | *Late D2* | *Poss. early D2* |
| | **A2173** | Cores mostly zoned prismatic, rarely homogeneous; Rims homogeneous | **1911±19** | **1822±7** | **1849±11** |
| | *Age interpretation* | | *Mixed protolith age* | *Late D2* | *Poss. early D2* |
| | **A2174** | Cores zoned prismatic, or homogeneous; Rims homogeneous | **1849±17** | **1818±12** | **1812±11** |
| | *Age interpretation* | | *Poss. early D2* | *Late D2* | *Late D2* |
| Mylonite | **A2175** | Cores mostly zoned prismatic, some homogeneous; Rims homogeneous | **1874±17** | **1790±12** | **1801±14** |
| | *Age interpretation* | | *Mixed protolith age* | *Late-orogenic retrograde SZ reactivation* | *Late-orogenic retrograde SZ reactivation* |

# 5. Interpretation: timing and style of shearing

The interpretation of the age determination results is summarised in Table 2.

*Zircon:* The zircon in the samples are typically prismatic with rims overgrowing the zoned cores, and the rims yield systematically younger ages of c. 1820–1810 Ma than the cores (Fig. 5a, Table 2, Electronic Appendix A). This, together with the observations of the high-T nature of the shearing in the granulite shear zone samples (A2170–A2174), the zircon cores are interpreted as inherited and probably magmatic; with the rims growing during the high-T shearing; in sample A2175, the young rim age of 1790 Ma is interpreted to represent the last (semi)ductile shearing phase along the SKFZ.

The effect of deformation on zircon (and titanite) growth and recrystallisation is only partially understood. It is usually assumed that especially zircon is stable during deformation and any effects to zircon rims result from prograde metamorphism that may or may not be synchronous with deformation. However, there are several indications that zircon rims may respond to deformation, particularly at high-T conditions: analytical studies have confirmed U-Pb system changes through recrystallisation and crystal-plastic deformation (e.g. Reddy et al. 2006; Piazolo et al. 2012), although how exactly age data from deformed zircon rims should be interpreted is still somewhat unclear. Nevertheless, zircon in post-peak metamorphism shear zones (i.e. after the phase where one would normally expect growth of zircon rims/new zircon

and new titanite) commonly show rim ages much younger than the age of the regional peak thermal event (e.g. Reddy et al. 2006; Piazolo et al. 2012). This suggests that zircon does directly respond to deformation in high-grade shear zones and, therefore, the rims can subsequently get modified during shearing resulting in younger U-Pb ages.

Comparison with other age determination results in Southern Finland shows that the c. 1820–1810 Ma ages obtained from the zircon rims within the pyroxene-bearing shear zones coincide with the youngest migmatite leucosome ages (Fig. 3 and references therein). In the study area, these migmatites were formed under granulite facies conditions (750–800°C and 4–5 kbar; Mouri et al. 2005) The microstructures defining the strong foliation within the pyroxene-bearing shear zones are dominantly those of high-temperature deformation, and the lack of pervasive retrogression supports the interpretation of deformation in high-T (at least amphibolite facies) conditions (Fig. 4b). To summarise, we interpret that the ages of c. 1820–1810 Ma, obtained from zircon rims, constrain the age of the shearing along the pyroxene shear zones during the last stages of the regional high-T peak metamorphism.

The age of 1800–1790 Ma of the approximately greenschist facies shearing along the Somero-Karkkila fault zone (sample A2175), however, does not coincide with any known thermal event. Based on the discussion above on the possible effect of deformation on the zircon U-Pb system, we interpret that this age reflects the late-orogenic retrograde deformation/re-activation along this shear zone. The age fits well with published age data on late-Fennian greenschist to lower amphibolite facies deformation e.g. along the crustal-scale SJSZ in the SW archipelago (Fig. 1; Torvela et al. 2008) and in Kimito area, NW of Hanko (Fig. 1; Levin et al. 2005).

*Titanite:* The titanite data is more complicated in terms of the Fennian ages. Three of the high-T shear zone titanite samples show 1850–1845 Ma ages, one shows a 1812 Ma age, and the SKFZ sample gives an age of 1801 Ma. Particularly the older titanite ages are difficult to interpret in the light of all other data. As the data from the zircon cores imply that the protolith ages for all samples is much older than the oldest titanite ages, we suggest that the 1850–1845 Ma titanite in samples A2170, A2171 and A2173 are inherited, and may represent either a mixed age or reflect a temporary cooling below the titanite U-Pb closure temperature, possibly due to the c. 1.85 Ga extensional event described by e.g. Bergman et al. (2008), Lahtinen & Nironen (2010) and Nironen & Mänttäri (2012). On the contrary, the 1812 Ma titanite U-Pb age of sample A2174 is very similar to the zircon rim age from this sample and is therefore, similarly to the zircon data, reliably interpreted as the age of late-Fennian shearing along this pyroxene-bearing shear zone.

The youngest titanite age of 1801 Ma from the greenschist facies SKFZ sample A2175 agrees well with the zircon rim age from that sample and therefore gives the age of the retrograde deformation phase along the SKFZ.

The field relationships between the sampled px-bearing shear zones (Fig. 4a, b) and the surrounding paragneisses and migmatites are not directly observable due to the contact zones being diffuse and covered by Quaternary deposits. The drag of the surrounding migmatitic foliations at a km-scale in the field and in seismic reflection data imply that these strongly deformed zones have an extensional kinematic component; the shear zones have previously been interpreted to reflect approximately orogen-parallel syn-convergent escape of the lower crust (see Torvela et al. 2013 for more information on the kinematic interpretations). The weak mineral lineation, observed at two sample locations (A2171 and A2173), plunge moderately toward NE, similar to the lineation patterns observed in the wider area (Figs. 4a, c). The lineations are interpreted to reflect the shear zone slip direction so that the E-W striking, north-dipping shear zones exhibit oblique, top-to-NE extension, whereas the c. NE-SW striking, SE-dipping shear zones show oblique, top-to-E extension (Fig. 6). The structural characteristics of the shear zones are representative

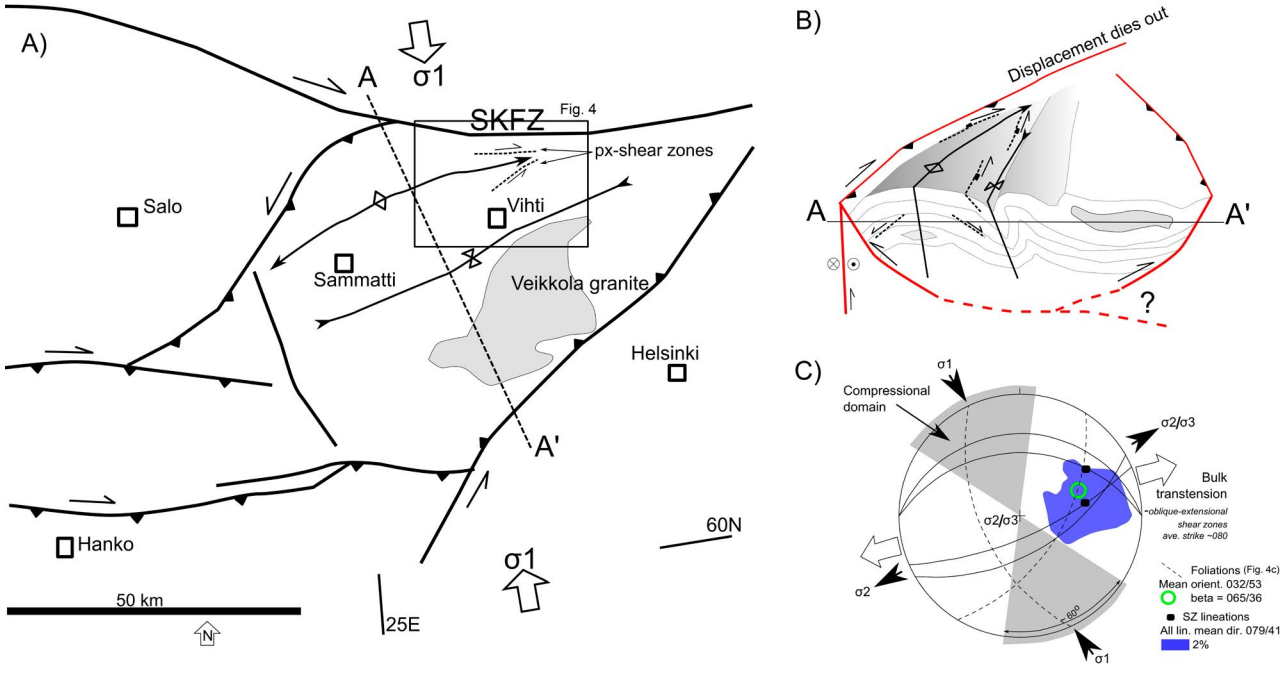


Figure 6. Schematic structural synthesis for the West Uusimaa Complex (WUC). a) Generalised fault and fold trend map of the WUC. Locations of the more detailed map in Fig. 2 and the cross section line in B) are shown. b) Schematic 3D block diagram, approximately to scale, showing the interpretation of the WUC as a laterally stretched pop-up structure within the transpressional Fennian tectonic framework. In this interpretation, the transtensional px-bearing shear zones are explained as local accommodation features within the flanks of the evolving large-scale anticlines/elongate domes, especially towards the 'tips' of domes where the domes start to pinch out: this is illustrated in c) Kinematic synthesis of the relationship between the overall compression and lateral stretching. The transtensional shear zones dated in this study and their associated stretching lineations, where observable, are drawn with solid great circles and black rectangles, respectively. The 2% density contour for the stretching lineations are also shown; the migmatite foliations and the mean fold axial plane orientation defined by the foliations are drawn with dashed great circles. We interpret that at the time of the formation of the shear zones, lateral escape within the dome was enabled by i) a temporary increase in the ratio σ1/σ2 from a near plane-strain relationship where σ2 is 'neutral'; or, more likely ii) a transient 'flip' of σ2 (or possibly even σ1) to subvertical at around 1.82 Ga as a result of the locally increased gravitational potential caused by the pop-up of this crustal block (see also Fossen & Tikoff, 1998 for models of spreading/transtension under overall transpression). See text for further discussion.

of the large-scale structural patterns of the Vihti area: the shear zone foliations and the lineations (where observed) correspond well with those observed within the WUC (Fig. 4c). The absence of cross-cutting relationships between the shear zones and the regional fabrics strongly suggests that the shear zones are genetically related to the overall crustal fabrics. The interpreted deformation ages of c. 1820–1815 Ma obtained in this study confirm their timing as syn-convergent. Therefore, the present study refines the interpretation of Torvela et al. (2013) to suggest that, based on the association of the shear zones with the large-scale fold flanks, there may be a relationship between the folds at various crustal levels and the transtensional shear zone formation (Fig. 6). Other low-angle shear zones might exist in a similar setting farther west: the flanks of the non-cylindrical large-scale fold ('dome') north of Sammatti, for example, may have been extensionally sheared during D2, although this is yet to be tested in the field (Torvela & Kurhila 2020).

To summarise, we interpret the age data combined with the field observations to reflect i) ~1820–1810 Ma syn-orogenic transtension along the high grade, shear zones facilitating (local?)

lateral escape (see Discussion); and ii) a late-stage ~1790 Ma (semi)ductile shearing along the Somero-Karkkila fault zone under (upper) greenschist facies conditions.

# 6. Discussion

The post -1.85 Ga orogenic compression and the associated prograde metamorphism and deformation in Southern Finland was coeval with the large-scale migmatisation and the formation of the microcline anatectic granite sheets (Fig. 3; e.g. Suominen 1991; Väisänen et al. 2002; Ehlers et al. 2004; Mouri et al. 2005; Kurhila et al. 2005; Nironen and Kurhila 2008; Skyttä & Mänttäri 2008; Kurhila et al. 2011). The syn-melt crustal shortening was dominantly accommodated by pervasive, crustal-scale open to tight folding with some thrusting (Torvela & Kurhila 2020). This overall compressional deformation style evolved, at least locally, around 1820–1815 Ma into transpression with syn-convergent lateral escape, producing local transtension along suitably orientated fold limbs such as those in the Vihti-Karkkila area (Fig. 6). The transtension and lateral escape would necessitate a (local) increase of the vertical stresses, possibly with a flip of $\sigma_2$ (or even $\sigma_1$) into subvertical (Fig. 6c). Further research is required to determine whether such features are common within the entire migmatitic middle crust; our model may be only locally applicable and related to the interpreted pop-up lens that forms the present West Uusimaa Complex (WUC; Fig. 6b). Lateral escape facilitated by a network of high-grade shear zones may also enable the formation of the 'dome-and-basin' geometry within WUC without the need to invoke a post-Fennian E-W 'Nordic compression' as suggested by Lahtinen et al. (2005). Fennian compression continued until at least 1.80–1.79 Ga as evidenced by the obtained ages within the SKFZ; therefore, the ~1.81–1.82 Ga transtensional shear zones are not evidence of a cessation of the orogenic compression regionally.

Skyttä and Mänttäri (2008) propose a "break" in compressional deformation, resulting in regional crustal extension at c. 1835–1825 Ma to explain the crustal-scale migmatisation and the foliation-parallel boudinage and other "flattening" structures near Orijärvi (south of Sammatti in Fig. 1). Whilst a local flattening scenario is possible, we consider that the foliation-parallel extension/flattening structures need not reflect crustal-scale dynamics, and extensional features can be local and transient in nature, as interpreted in the WUC. However, there is still insufficient data across the LSGM to define whether the extensional features reflect large-scale crustal dynamics or merely local, transient accommodation of strain. If the shear zones reflect large-scale extension, the suggestion by e.g. Nironen (1997) that the migmatisation of the Fennian middle crust was caused by rapid exhumation due to orogenic collapse and extension is not supported by our results. The transtensional shear zones accommodating lateral escape (and possibly enabling the first stages of significant exhumation) are synchronous or slightly post-date peak metamorphism. If the extension is more local, as the results of this study preferentially imply, the presence of the extensional or transtensional shear zones must be interpreted with caution as extensional features can form at all scales within an overall compressional stress regime, particularly towards the later stages of an orogen (see also Ferrill et al. 2021). This has also been the conclusion of e.g. Chardon et al. (2011) whose overall kinematic model for the deformation of hot orogenic crust is partly similar to ours.

Relatively little is known about SKFZ, but similarly to the Sottunga-Jurmo Shear Zone (SJSZ) in the Åland archipelago (Fig. 1; Torvela et al. 2008), it seems to be a long-lived feature. Field observations indicate that there is at least one, possibly dextral, phase of shearing at a high-grade (at least upper amphibolite facies), represented by the steep, E-W striking gneissose foliations shown in Fig. 4a. The age of this gneissose shearing phase is unknown. The last (semi-)ductile, apparently dextral (Fig. 4b)

phase at greenschist facies conditions is dated in this study at 1.80–1.79 Ga. This age agrees well with other ages and observations across LSGM that the entire area had reached lower amphibolite to greenschist facies conditions by about 1.80 Ga, with deformation partitioned almost exclusively into steep strike-slip shear zones (e.g. Lindroos et al. 1996; Lahtinen et al. 2005; Levin et al. 2005; Mouri et al. 2005; Torvela et al. 2008). The SKFZ does not seem to be as extensive as the SJSZ, and can be traced with confidence only for about 80 km and the shear zone seems to die out together with the WUC in the east (Fig. 6a, b). The cross section across this area does imply that there may be several km of syn-Fennian vertical motion along the SKFZ, although the amount of vertical displacement during the post-Fennian greenschist facies deformation is unclear (Torvela & Kurhila 2020).

To summarise, the new age data combined with the structural information on both local and regional scale further constrain the timing of the changes in the crustal deformation style during orogenesis from; i) high-grade, compression-dominated to similarly high-grade but combined transpression – lateral stretching and escape at ~1.82 Ga, and to ii) the late- to post-orogenic transition into retrograde conditions with dominantly strike-slip shearing at ~1.80–1.79 Ga. We envisage that the first transition resulted from the prolonged transpression building a thickened, internally complex crustal configuration; this, at least locally, allowed the formation of sufficient gravitational potential to enable transtension and lateral escape of the high-grade middle crust. Whether such transtension was penetrative throughout the migmatitic crust of Southern Finland remains an open question, but according to our model the 1.82–1.81 Ga transtension may have been a local and transient feature.

# Acknowledgements

We are grateful to Yann Lahaye for the help with the LA-ICPMS measurements; and to Henrik Kalliomäki for the sample preparation for the age determinations. Many thanks also to Annakaisa Korja for introducing the West Uusimaa area, to K.H. Renlunds Stiftelse and Academy of Finland consortium project "Three dimensional evolution of the middle crust in Central Fennoscandia" for funding the fieldwork in this area. We thank Joel Andresson and Karin Högdahl for their thorough reviews and Niina Kuosmanen for the editorial work.

# Supplementary Data

Electronic Appendix A for this article are available via Bulletin of the Geological Society of Finland web page.
Electronoc Appendix A: LA-MC-ICPMS analysis results.

# References

Andersen, T., Griffin, W. L., Jackson, S. E., Knudsen, T.-L. & Pearson, N. J. 2004. Mid-Proterozoic magmatic arc evolution at the southwest margin of the Baltic Shield. Lithos 73, 289–318. https://doi.org/10.1016/j.lithos.2003.12.011

Belousova, E. A., Griffin, W. L. & O'Reilly, S. Y., 2006. Zircon crystal morphology, trace element signatures and Hf isotope composition as a tool for petrogenetic modeling: examples from Eastern Australian granitoids. Journal of Petrology 47, 329–353. https://doi.org/10.1093/petrology/egi077

Bergman, S., Högdahl, K., Nironen, M., Ogenhall, E., Sjöström, H., Lundqvist, L. & Lahtinen, R., 2008. Timing of Palaeoproterozoic intra-orogenic sedimentation in the central Fennoscandian Shield; evidence from detrital zircon in metasandstone. Precambrian Research 161, 231–249. https://doi.org/10.1016/j.precamres.2007.08.007

Bleeker, W. & Westra, L., 1987. The evolution of the Mustio gneiss dome, Svecofennides of SW Finland. Precambrian Research 36, 227–240. https://doi.org/10.1016/0301-9268(87)90022-2

Cagnard, F., Gapais, D. & Barbey, P., 2007. Collision tectonics involving juvenile crust: The example of the southern Finnish Svecofennides. Precambrian Research 154, 125–141. https://doi.org/10.1016/j.precamres.2006.12.011

Chardon, D., Jayananda, M. & Peucat, J-J., 2011. Lateral constructional flow of hot orogenic crust: insights from the Neoarchaean of south India, geological and geophysical implications for orogenic plateaux. Geochemistry, Geophysics, Geosystems 12, Doi: 10.1029/2010GC003398.

Ehlers, C., Lindroos, A. & Selonen, O., 1993. The late Svecofennian granite-migmatite zone of southern Finland – a belt of transpressive deformation and granite emplacement. Precambrian Research 64, 295–309. https://doi.org/10.1016/0301-9268(93)90083-E

Ehlers, C., Skiöld, T. & Vaasjoki, M. 2004. Timing of Svecofennian crustal growth and collisional tectonics in Åland, SW Finland. Bulletin of the Geological Society of Finland 76, 63–91. https://doi.org/10.17741/bgsf/76.1-2.004

Eklund, O. & Shebanov, A., 2005. Prolonged postcollisional shoshonitic magmatism in the southern Svecofennian domain – a case study of the Åva granite-lamprophyre ring complex. Lithos 80, 229–247. https://doi.org/10.1016/j.lithos.2004.06.012

England, P. & Houseman, G., 1989. Extension during continental convergence, with application to the Tibetan Plateau. Journal of Geophysical Research 94, 17561–17579. https://doi.org/10.1029/JB094iB12p17561

Ferrill, D. A., Smart, K. J., Cawood, A. J., & Morris, A. P., 2021. The fold-thrust belt stress cycle: Superposition of normal, strike-slip, and thrust faulting deformation regimes. Journal of Structural Geology 148, doi:10.1016/j.jsg.2021.104362.

Fossen, H. & Tikoff, B., 1998. Extended models of transpression and transtension, and application to tectonic settings. In: Holdsworth, E.R., Strachan, R.A. & Dewey, J.D. (Eds.). Continental Transpressional and Transtensional Tectonics. Geological Society London, Special Publication 132, 15–33. https://doi.org/10.1144/GSL.SP.1998.135.01.02

Goldsmith, J. R. & Newton, R. C., 1977. Scapolite-plagioclase stability relations at high pressures and temperatures in the system $NaAlSi_3O_8$-$CaAl_2SI_2O_2$-$CaCO_3$-$CaSO_4$. American Mineralogist 62, 1063–1081.

Hermansson, T., Stephens, M. B., Corfu, F., Andersson, J. & Page, L., 2007. Penetrative ductile deformation and amphibolite-facies metamorphism prior to 1851 Ma in the western part of the Svecofennian orogen, Fennoscandian Shield. Precambrian Research 153, 29–45. https://doi.org/10.1016/j.precamres.2006.11.009

Hiltunen, A., 1982. The Precambrian geology and skarn iron ores of the Rautuvaara area, northern Finland. Geological Survey of Finland, Bulletin 318. 133 p.

Högdahl, K., Sjöström, H., Andersson, U. B. & Ahl, M., 2008. Continental margin magmatism and migmatisation in the west-central Fennoscandian Shield. Lithos 102, 435–459. https://doi.org/10.1016/j.lithos.2007.07.019

Huhma, H., Mänttäri, I., Peltonen, P., Kontinen, A., Halkoaho, T., Hanski, E., Hokkanen, T., Hölttä, P., Juopperi, H., Konnunaho, J., Lahaye, Y., Luukkonen, E., Pietikäinen, K., Pulkkinen, A., Sorjonen-Ward, P., Vaasjoki, M. & Whitehouse, M., 2012. The age of the Archaean greenstone belts in Finland. Geological Survey of Finland, Special Paper 54, 74–174.

Jackson S. E., Pearson N. J., Griffin W. L. & Belousova E. A., 2004. The application of laser ablation-inductively coupled plasma-mass spectrometry to in-situ U–Pb zircon geochronology. Chemical Geology 211, 47–69. https://doi.org/10.1016/j.chemgeo.2004.06.017

Johannes, W., Ehlers, C., Kriegsman, L. M. & Mengel, K., 2003. The link between migmatites and S-type granites in the Turku area, southern Finland. Lithos 68, 69–90. https://doi.org/10.1016/S0024-4937(03)00032-X

Jurvanen, T., Eklund, O. & Väisänen, M., 2005. Generation of A-type granitic melts during late Svecofennian metamorphism in southern Finland. Geologiska Föreningen i Stockholms Förhadlingar 127, 139–147. https://doi.org/10.1080/11035890501272139

Korsman, K., Koistinen, T., Kohonen, J., Wennerström, M., Ekdahl, E., Honkamo, M., Idman, H. & Pekkala, Y. (eds) 1997. *Bedrock Map of Finland 1:1000000*. Geological Survey of Finland.

Kurhila, M., Vaasjoki, M., Mänttäri, I., Rämö, T. & Nironen, M., 2005. U-Pb ages and Nd isotope characteristics of the lateorogenic, migmatizing microcline granites in southwestern Finland. Bulletin of the Geological Society of Finland 77, 105–128. https://doi.org/10.17741/bgsf/77.2.002

Kurhila, M., Mänttäri, I., Vaasjoki, M., Rämö, O.T. & Nironen, M., 2011. U-Pb geochronological constraints of the late Svecofennian leucogranites of southern Finland. Precambrian Research 190, 1–24. https://doi.org/10.1016/j.precamres.2011.07.008

Lahtinen, R. & Huhma, H., 1997. Isotopic and geochemical constraints on the evolution of the 1.93-1.79 Ga Svecofennian crust and mantle in Finland. Precambrian Research 82, 13–34. https://doi.org/10.1016/S0301-9268(96)00062-9

Lahtinen, R. & Nironen, M., 2010. Paleoproterozoic lateritic paleosol–ultra-mature/mature quartzite–meta-arkose successions in southern Fennoscandia—intra-orogenic stage during the Svecofennian orogeny. Precambrian Research 183, 770–790. https://doi.org/10.1016/j.precamres.2010.09.006

Lahtinen, R., Korja, A. & Nironen, M., 2005. Palaeoproterozoic tectonic evolution. In: Lehtinen, M., Nurmi, P. A. & Rämö, O.T. (eds.) Precambrian Geology of Finland – Key to the Evolution of the Fennoscandian Shield. Developments in Precambrian Geology 14, 481–532.

Latvalahti, U., 1979. Cu–Zn–Pb ores in the Aijala-Orijärvi area, South-west Finland. Economic Geology 79, 1035–1059. https://doi.org/10.2113/gsecongeo.74.5.1035

Levin, T., Engström, J., Lindroos, A., Baltybaev, S. & Levchenkov, O., 2005. Late-Svecofennian transpressive deformation in SW Finland – evidence from late-stage D3 structures. Geologiska Föreningen i Stockholms Förhadlingar 127, 129–137. https://doi.org/10.1080/11035890501272129

Lindroos, A., Romer, R.L., Ehlers, C. & Alviola, R., 1996. Late-orogenic Svecofennian deformation in SW Finland constrained by pegmatite emplacement ages. Terra Nova 8, 567–574. https://doi.org/10.1111/j.1365-3121.1996.tb00786.x

Ludwig, K.R., 2003. Isoplot/Ex 3.00: A geochronological toolkit for Microsoft Excel: Berkeley Geochronology Center Special Publication 4.

Mouri, H., Väisänen, M., Huhma, H. & Korsman, K., 2005. Sm-Nd garnet and U-Pb monazite dating of high-grade metamorphism and crustal melting in the West Uusimaa area, southern Finland. Geologiska Föreningen i Stockholms Förhadlingar 127, 123–128. https://doi.org/10.1080/11035890501272123

Müller, W., M. Shelley, Miller, P. & Broude, S., 2009. Initial performance metrics of a new custom-designed ArF excimer LA-ICPMS system coupled to a two-volume laser-ablation cell. Journal of Analytical Atomic Spectrometry 24, 209–214. Doi: 10.1039/B805995K

Nironen, M., 1997. The Svecofennian orogen: a tectonic model. Precambrian Research 86, 21–44. https://doi.org/10.1016/S0301-9268(97)00039-9

Nironen, M. & Kurhila, M., 2008. The Veikkola granite area in southern Finland: emplacement of a 1.83-1.82 Ga plutonic sequence in an extensional regime. Bulletin of the Geological Society of Finland 80, 39–68. https://doi.org/10.17741/bgsf/80.1.003

Nironen, M. & Mänttäri, I., 2012. Timing of accretion, intra-orogenic sedimentation and basin inversion in the Paleoproterozoic Svecofennian orogen: the Pyhäntaka area, southern Finland. Precambrian Research 192–195, 34–51. https://doi.org/10.1016/j.precamres.2011.09.013

Nironen, M., Mänttäri, I. & Väisänen, M., 2016. The Salittu Formation in southwestern Finland, part I: Structure, age and stratigraphy. Bulletin of the Geological Society of Finland 88, 85–103. https://doi.org/10.17741/bgsf/88.2.003

Pajunen, M., Airo, M.-L., Elminen, T., Mänttäri, I., Niemelä, R., Vaarma, M., Wasenius, P. & Wennerström, M., 2008. Tectonic evolution of the Svecofennian crust in southern Finland. In: Pajunen, M. (ed.). Tectonic evolution of the Svecofennian crust in southern Finland – a basis for characterizing bedrock technical properties. Geological Survey of Finland, Special Paper 47, 15–161.

Patchett, J. & Kouvo, O., 1986. Origin of continental crust of 1.9-1.7 Ga age: Nd isotopes and U-Pb zircon ages in the Svecokarelian terrain of south Finland. Contributions to Mineralogy and Petrology 92, 1–12. https://doi.org/10.1016/0301-9268(87)90050-7

Piazolo, S., Austerheim, H. & Whitehouse, M., 2012. Brittle-ductile microfabrics in naturally deformed zircon: Deformation mechanisms and consequences for U-Pb dating. American Mineralogist 97, 1544–1563. https://doi.org/10.2138/am.2012.3966

Reddy, S. M., Timms N. E., Trimby, P., Kinny, P. D., Buchan, C. & Blake, K., 2006. Crystal-plastic deformation of zircon: A defect in the assumption of chemical robustness. Geology 34, 257–260. https://doi.org/10.1130/G22110.1

Rosa D. R. N., Finch A. A., Andersen T. & Inverno C. M. C., 2009. U-Pb geochronology and Hf isotope ratios of magmatic zircons from the Iberian pyrite belt. Mineralogy and Petrology 95, 47–69. Doi: 10.1007/s00710-008-0022-5

Saalmann, K., Mänttäri, I., Ruffet, G. & Whitehouse, M. J., 2009. Age and tectonic framework of structurally controlled Palaeoproterozoic gold mineralization in the Häme belt of southern Finland. Precambrian Research 174, 53–77. https://doi.org/10.1016/j.precamres.2009.06.005

Sanderson, D. J. & Marchini, W. R. D., 1984. Transpression. Journal of Structural Geology 6, 449–458. https://doi.org/10.1016/0191-8141(84)90058-0

Schreurs, J. & Westra, L., 1986. The thermotectonic evolution of a Proterozoic, low pressure, granulite dome, West Uusimaa, SW Finland. Contributions to Mineralogy and Petrology 93, 236–250. https://doi.org/10.1007/BF00371326

Selonen, O., Ehlers, C. & Lindroos, A., 1996. Structural features and emplacement of the late Svecofennian Perniö granite sheet in southern Finland. Bulletin of the Geological Society of Finland 68, 5–17. https://doi.org/10.17741/bgsf/68.2.001

Skyttä, P. & Mänttäri, I., 2008. Structural setting of late Svecofennian granites and pegmatites in Uusimaa Belt, SW Finland: Age constraints and implications for crustal evolution. Precambrian Research 164, 86–109. https://doi.org/10.1016/j.precamres.2008.04.001

Skyttä, P., Väisänen, M. & Mänttäri, I., 2006. Preservation of Palaeoproterozoic early Svecofennian structures in the Orijärvi area, SW Finland – Evidence for polyphase strain partitioning. Precambrian Research 150, 153–172. https://doi.org/10.1016/j.precamres.2006.07.005

van Staal, C. R. & Williams, P. F., 1983. Evolution of a Svecofennian-mantled gneiss dome in SW Finland, with evidence for thrusting. Precambrian Research 21, 101–128. https://doi.org/10.1016/0301-9268(83)90007-4

Stacey, J. S. & Kramers, J. D. 1975 Approximation of terrestrial lead isotope evolution by a two-stage model. Earth and Planetary Science Letters 26, 207–221. https://doi.org/10.1016/0012-821X(75)90088-6

Stålfors, T. & Ehlers, C., 2005. Emplacement mechanisms of lateorogenic granites: structural and geochemical

evidence from southern Finland. International Journal of Earth Science 95, 557–568. https://doi.org/10.1007/s00531-005-0049-3

Steiger, R. H & Jäger, E., 1977. Subcommission on geochronology – convention on the use of decay constants in geochronology and cosmochronology. Earth and Planetary Science Letters 36, 359–362. https://doi.org/10.1016/0012-821X(77)90060-7

Suominen, V., 1991. The chronostratigraphy of southwester Finland with special reference to Postjotnian and Subjotnian diabases. Geological Survey of Finland, Bulletin 356, 1–100.

Torvela, T. & Annersten, H., 2005. PT-conditions of deformation within the Palaeoproterozoic South Finland shear zone: some geothermobarometric results. Bulletin of the Geological Society of Finland 77, 151–164. https://doi.org/10.17741/bgsf/77.2.004

Torvela, T. & Ehlers, C. 2010a. Microstructural associated with the Sottunga-Jurmo shear zone and their implications to the 1.83-1.79 Ga tectonic development of SW Finland. Bulletin of the Geological Society of Finland 82, 5–29. https://doi.org/10.17741/bgsf/82.1.001

Torvela, T. & Ehlers, C., 2010b. From ductile to brittle deformation – structural development and strain distribution along a crustal-scale shear zone in SW Finland. International Journal of Earth Science 99, 1133–1152. https://doi.org/10.1007/s00531-009-0451-3

Torvela, T. & Kurhila, M., 2020. How does the orogenic crust deform? Evidence of crustal-scale competent behaviour of partially molten middle crust during orogenic compression. Precambrian Research 342. https://doi.org/10.1016/j.precamres.2020.105670

Torvela, T., Mänttäri, I. & Hermansson, T., 2008. Timing of deformation phases within the South Finland shear zone, SW Finland. Precambrian Research 160, 277–298. https://doi.org/10.1016/j.precamres.2007.08.002

Torvela, T., Moreau, J., Butler, R. W. H., Korja, A. & Heikkinen, P., 2013. The mode of deformation in the orogenic mid-crust revealed by seismic attribute analysis. Geochemistry, Geophysics, Geosystems 14, 1069–1086. https://doi.org/10.1002/ggge.20050

Väisänen, M. & Hölttä, P., 1999. Structural and metamorphic evolution of the Turku migmatite complex, southwestern Finland. Bulletin of the Geological Society of Finland 71, 177–218. https://doi.org/10.17741/bgsf/71.1.009

Väisänen, M. & Mänttäri, I., 2002. 1.90–1.88 Ga primitive arc, mature arc and back-arc basin in the Orijärvi area, SW Finland. Bulletin of the Geological Society of Finland 74, 185–214. https://doi.org/10.17741/bgsf/74.1-2.009

Väisänen, M. & Skyttä, P., 2007. Late Svecofennian shear zones in southwestern Finland. Geologiska Föreningen i Stockholms Förhadlingar 129, 55–64. https://doi.org/10.1080/11035890701291055

Väisänen, M., Mänttäri, I., Kriegsman, L. M. & Hölttä, P., 2000. Tectonic setting of post-collisional magmatism in the Palaeoproterozoic Svecofennian Orogen, SW Finland. Lithos 54, 63–81. https://doi.org/10.1016/S0024-4937(00)00018-9

Väisänen, M., Mänttäri, I. & Hölttä, P., 2002. Svecofennian magmatic and metamorphic evolution in southwestern Finland as revealed by U-Pb zircon SIMS geochronology. Precambrian Research 116, 111–127. https://doi.org/10.1016/S0301-9268(02)00019-0